Magnetic-field dependent Andreev reflection in narrow Nb/InAs Josephson junctions

F. Rohlfing,[1] G. Tkachov,[2,*] F. Otto,[1] K. Richter,[2] D. Weiss,[1] G. Borghs,[3] and C. Strunk[1]

[1]*Institute for Exp. and Applied Physics, Universität Regensburg, D-93040 Regensburg, Germany*
[2]*Institute for Theoretical Physics, Universität Regensburg, D-93040 Regensburg, Germany*
[3]*Interuniversity Micro-Electronics Center (IMEC), Kapeldreef 75a, B-3001 Leuven, Belgium*

We study narrow ballistic Josephson weak links in an InAs quantum well contacted by Nb electrodes. Measurements of the conductance, excess and critical currents reveal a dramatic magnetic-field suppression of the Andreev reflection amplitude, which occurs even for in-plane field orientation with essentially no magnetic flux through the junction. Our observations demonstrate the presence of an additional energy scale in the spectrum of the hybrid Nb/InAs-banks and the effect of screening currents in them.

PACS numbers: 74.45.+c, 74.50.+r, 74.81.-g, 85.25.Cp

In recent years a detailed microscopic understanding of the proximity effect has emerged. There is now agreement that in highly transparent Josephson junctions formed by a metallic weak link in good contact with two superconducting (SC) banks the supercurrent is carried by Andreev bound states (ABS)[1]. The latter come in pairs corresponding to the opposite directions of Cooper-pair transfer mediated by multiple Andreev reflection (MAR) at the superconductor/metal interfaces provided that the acquired quasi-particle phase is a multiple of 2π.[2] At currents exceeding the critical current $I_C(T, B)$ MAR between the two SC banks manifests itself in the current-voltage characteristics as subharmonic gap structures at voltages $eV_n = 2\Delta/n$, where Δ is the SC energy gap and $n = 1, 2, \ldots$. At higher voltage $eV \gg 2\Delta$, $I(V)$ becomes linear with an excess current $I_{\rm exc} = I(V) - G_N V$ determined by a single Andreev reflection (AR) probability $|a(\varepsilon)|^2$ (G_N is the normal state conductance).[3,4]

Weak links formed by a two-dimensional electron gas (2DEG) in a semiconductor quantum well[5] are of particular interest because here the ballistic transport regime can be studied. In very high magnetic field perpendicular to the 2DEG, theory[6] and experiments[7,8] have demonstrated Andreev transport via edge-states. Indirect evidence for a strong magnetic-field effect on AR was experimentally found in AR antidot billiards.[9] The case of parallel field, with respect to the 2DEG, is equally intriguing: as ideally no magnetic flux threads the 2DEG, one may naively expect the Josephson current to survive up to the critical fields of the SC leads. This is not the case, but the underlying mechanism of the supercurrent suppression is still unclear. This question, also relevant for other 2D hybrid systems,[10] is among the issues this study focuses on.

In this Communication, Nb/InAs Josephson junctions of different width are studied in a four-terminal lead configuration within the 2DEG. This allows us to separately determine the transparencies of the InAs weak link and the Nb/InAs-interface, and identify an additional energy scale appearing in the electronic structure of the hybrid SC terminals. We observe a very strong suppression of both the AR probability and supercurrent in weak magnetic fields of 4 and 100 mT for perpendicular and parallel orientations, respectively. This unexpectedly rapid decay can be traced back to the diamagnetic supercurrents in the Nb, which break the time-reversal symmetry of the AR process for both field orientations.

The samples were prepared from a heterostructure containing an InAs-quantum well with thickness $d_N = 15\,$nm and a mean free path around 3.7 μm, confined between two AlGaSb layers. The electron density was $7.8 \cdot 10^{15}\,\mathrm{m}^{-2}$, resulting in a Fermi wavelength $\lambda_F = 2\pi/k_F = 28\,$nm.[7] First, a constriction of width W with a four-terminal (4t) lead structure (shown in yellow in Fig. 1a) was patterned using electron beam lithograpy (EBL) and etched by reactive ion etching in a $SiCl_4$-plasma. In a second EBL step two Nb stripes were deposited onto the InAs (horizontal grey bars in Fig. 1a) after removal of the top AlGaSb layer and in-situ Ar-ion cleaning of the InAs surface. The Nb-stripes have a width $W_S = 1\,\mu$m and a thickness $d_S = 35\,$nm; their distance $L = 600\,$nm defines the length L of the junction. This results in a Thouless energy of $\varepsilon_{Th} = \hbar v_F/L = 0.8\,$meV $\lesssim \Delta$ for all samples, v_F being the Fermi velocity in the normal metal. We have prepared four samples on two chips in the same batch. The chips contained junctions with $W = 0.5$ and $1\,\mu$m (denoted as #1 and #2a), and $W = 1$ and $2\,\mu$m (denoted #2b and #3), respectively.

Figure 1b shows the two-terminal (2t) resistance of samples #1, #2a, and #3 measured through the Nb stripes vs. temperature T. The resistance drops at the transition temperature of the Nb stripes around 8.3 K and again between 2 and 3 K, where the constriction becomes superconducting. In Fig. 1c we plot the 2t-resistance measured across the Nb stripes and the 4t-resistance measured within the InAs layer at $T = 10\,$K as a function of W. The 4t-resistance scales as $1/W$, obeying the ballistic Landauer-Büttiker formula:

$$G_N = \frac{2e^2}{h} \sum_n \mathcal{T}_n = \frac{2e^2}{h} \frac{k_F W}{\pi} \cdot \langle \mathcal{T} \rangle \,, \qquad (1)$$

where $\langle \mathcal{T} \rangle$ is the average channel transparency. From the slope of $G_N(W)$ we extract $\langle \mathcal{T} \rangle = 0.8$. The 2t-resistance

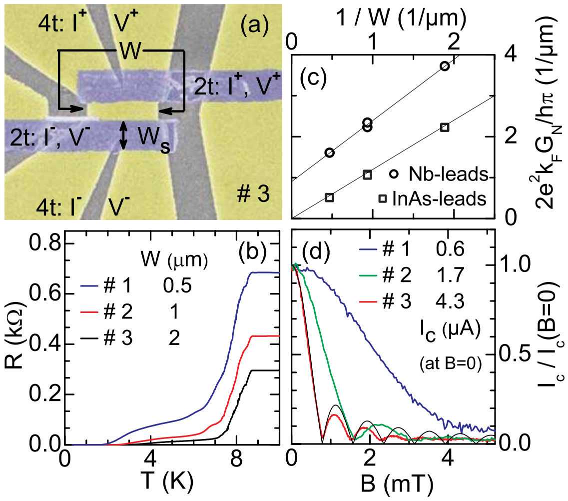

FIG. 1: a) Scanning electron micrograph of sample #3 with width $W = 2\,\mu$m and length $L = 0.6\,\mu$m. Regions containing the InAs two-dimensional electron gas are shown in yellow. Etched regions are light grey. The horizontal dark grey stripes are made from a 35 nm thick Nb. b) $R(T)$ for three samples with width $W = 0.5$, 1, $2\,\mu$m. c) Resistance at 10 K vs. $1/W$ for the 4t-configuration with InAs leads (O) and the 2t-configuration with Nb leads (□). d) Solid lines: normalized supercurrent I_C vs. transversal magnetic field $B_\perp$ for different values of W. The black line is the standard Fraunhofer pattern, fitted to the curve of sample #3 ($W = 2\,\mu$m).

at 10 K is also proportional to $1/W$, however, with an offset caused by the normal state resistance of the Nb-stripes and the Nb/InAs-interface resistance. Finally, we show in Fig. 1d the interference pattern of the junctions in a transversal magnetic field. For the widest junction the critical current $I_C(B)$ exhibits the expected Fraunhofer pattern.[11] For the narrower ones the higher order maxima are suppressed, and in the 0.5 μm-wide device $I_C(B)$ resembles more a Gaussian rather than a Fraunhofer pattern. This will be addressed below.

Information about the spectral distribution of ABS is contained in the T-dependence of the supercurrent. In Fig. 2 we present the critical current I_C at $B = 0$ as a function of temperature for different widths $W = 0.5$, 1 and $2\,\mu$m of the InAs constriction. With decreasing temperature $I_C(T)$ initially increases and then saturates at $T \lesssim 1$ K. The solid lines are fits based on the approach of Grajcar et al.[12] who adapted the scattering theory for the Josephson current[13] to 2D ballistic proximity structures. Two parameters were used in these fits: the average normal-state transmission probability $\langle\mathcal{T}\rangle$ and the McMillan energy $\Gamma_{McM} = \tau_{SN} \cdot \hbar v_F / 2d_N$,[14] which is the Thouless energy of the InAs quantum well multiplied by the Nb/InAs interface transparency τ_{SN}. Γ_{McM} determines the strength of the proximity-induced superconducting correlations in the InAs regions underneath the Nb film, which act as effective superconducting terminals described by the Green's functions of the McMillan model.[12,15] Clearly, the smaller τ_{SN}, the weaker the

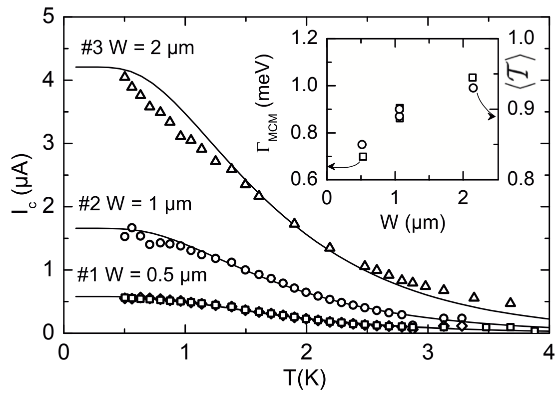

FIG. 2: Critical current vs. temperature T for different widths W together with best fits according to our model. Inset: Values of $\langle\mathcal{T}\rangle$ (O) and Γ_{McM} (□) resulting from the fits.

proximity effect. Because $\langle\mathcal{T}\rangle$ influences mainly the saturation value of $I_C(T \to 0)$, while Γ_{McM} determines the decay of I_C with T, these two parameters can be extracted independently from the measured $I_C(T)$.

The resulting fit parameters are presented in the inset of Fig. 2. The values for $\langle\mathcal{T}\rangle$ scatter by $\pm 5\,\%$ around 0.9, which is slightly higher, but still close to the value $\langle\mathcal{T}\rangle = 0.8$ estimated independently from the 4t-resistance (Eq. 1). The values of Γ_{McM} scatter by $\pm 15\,\%$ around 0.9 meV. From the latter value, we can estimate $\tau_{NS} \approx 0.06$, which is considerably smaller than $\langle\mathcal{T}\rangle$. The high mobility of the InAs-quantum well provides the high transparency of the constriction, while the comparatively low Nb/InAs interface transparency determines the additional energy scale Γ_{McM}.

Having all sample parameters fixed, we now turn to the main topic of our study, i.e. the magnetic field dependence of the AR amplitude. First, we focus on the IV- and dI/dV-characteristics. Figure 3 shows the differential conductance dI/dV of sample #2a ($W = 1\,\mu$m) for different values of magnetic field $B_\perp$ applied perpendicular to the sample. At $B_\perp = 0$ subharmonic gap structures (see arrows) appear at integer fractions $V_n = 2\Delta_{Nb}/ne$ of $2\Delta_{Nb}$. The location of the steps vs. $1/n$ is plotted in the inset of Fig. 3 and agrees very well with the value of $\Delta_{Nb} = 1.35$ meV. Only the step for $n = 1$ appears at lower voltage, a feature predicted in Ref. 16. Already a tiny perpendicular field of 4 mT washes out these steps. At 10 mT they vanish completely and also the low bias enhancement of dI/dV is gradually suppressed. It is known[2,17] that the subharmonic gap structure and the low bias enhancement of dI/dV originate from multiple AR at finite bias voltages. The large number of steps independently confirms the high AR probability $|a|^2$ expected from the high values of $\langle\mathcal{T}\rangle$. The rapid smearing of the steps thus indicates a surprisingly strong magnetic field dependence of $|a|^2$.

This observation is further substantiated by the behavior of the excess current $I_{\rm exc}$,[4] which is determined by

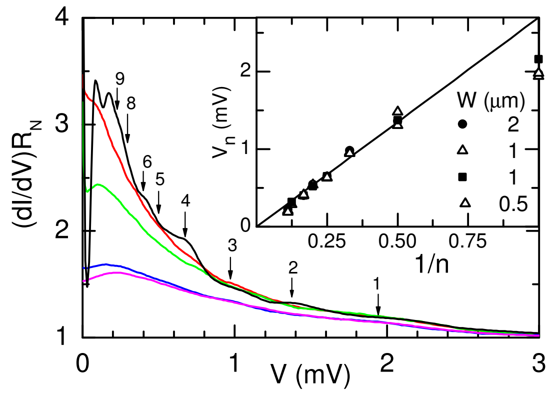

FIG. 3: (color online) Measured differential conductance dI/dV of sample #2a ($W = 1\mu$m) for different values of a perpendicular magnetic field $B_\perp = 0, 4, 10, 40$, and 100 mT, from top to bottom. Arrows indicate the subharmonic gap structure induced by multiple Andreev reflections. Inset: Voltages of the subharmonic gap structures for all samples. The solid line indicates the expected slope for $\Delta_{Nb} = 1.35$ meV.

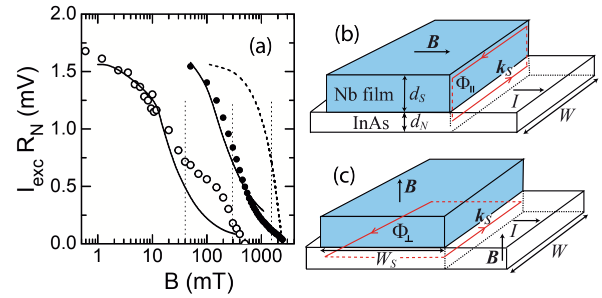

FIG. 4: (color online) (a) Measured excess current of sample #2a vs. perpendicular (∘) and parallel (•) magnetic field. The solid lines result from our model including the Doppler shift $\varepsilon_D(k_S)$ (see text) and the dashed line shows I_{exc} due to the suppression of $\Delta_{Nb}(B_\parallel)$ only.[18] (b) and (c) One of the Nb/InAs terminals in parallel and perpendicular fields. Red arrows indicate the SC order-parameter phase gradient, $\mathbf{k}_S = \nabla\gamma$, with $k_S = -\pi/W \times \Phi/\Phi_0$ determined by the magnetic flux Φ through the bilayer for given field orientation.

integrating $dI/dV - G_N$ (see Fig. 3) over voltage. Since I_{exc} results from a single AR if $V > 2\Delta_{Nb}$, it is more robust than the MAR-steps, whose amplitude is given by $|a|^{2n}$. Figure 4 shows I_{exc} on a logarithmic field scale for both field orientations. It is suppressed to ~ 50 % at $B_\perp = 30$ mT and $B_\parallel = 300$ mT. The field $B_\parallel$ exceeds $B_\perp$ by an order of magnitude, but is still a factor of 5 smaller than needed for an appreciable reduction of the gap $\Delta_{Nb}(B)$ as follows from the pair-breaking theory[18] (dashed line in Fig. 4).

We attribute the behavior of $I_{\text{exc}}(B)$ to the magnetic field suppression of the Andreev reflection in the InAs proximity regions underneath the Nb films. In the presence of the external field $\mathbf{B} = \nabla \times \mathbf{A}(\mathbf{r})$, the SC order parameter acquires an inhomogeneous phase, $\gamma(\mathbf{r}) = -2\pi\Phi_0^{-1}\int_{\mathbf{r}_0}^{\mathbf{r}} \mathbf{A}(\mathbf{r}')d\mathbf{r}'$, whose gradient $\mathbf{k}_S = \nabla\gamma$ induces diamagnetic currents in the entire Nb/InAs structure, including the InAs proximity layer (see, Fig. 4b and c). If $\mathbf{k}_i$ and $\mathbf{k}_f$ denote the wave vectors of initial and final quasi-particle states in the AR-process, momentum conservation requires $\mathbf{k}_i + \mathbf{k}_f = \mathbf{k}_S$, since the Cooper-pairs absorbed by the moving SC condensate have momentum $\hbar\mathbf{k}_S$. This leads to a *Doppler shift* $\varepsilon_D = -\hbar^2 k_\perp k_S/2m^*$ of the energy of the AR quasi-particle ($k_\perp$ is the transverse wave number).[19] The inset in Fig. 5 illustrates the energy dependence of $|a(\varepsilon)|^2$. It has two peaks, one at Δ_{Nb} and another at a smaller energy reflecting the hybrid nature of the superconducting Nb/InAs-bilayer. The suppression of $|a(\varepsilon)|^2$ occurs in the range $|\varepsilon| \lesssim \Gamma_{McM}$, when ε_D becomes comparable to the McMillan energy Γ_{McM}.[20]

The solid lines in Fig. 4a show $I_{\text{exc}}(B)$ obtained from the BTK-model,[4] in which we express the AR amplitude $a(\varepsilon)$ in terms of the McMillan's Green's functions[12,15] accounting for the Doppler shift ε_D in the InAs proximity layer. Using the parameters *extracted from Fig.* 2, the model reproduces the measured curves quite well (except for the shoulder in $I_{\text{exc}}(B_\perp)$, which at present is not understood). The model accounts for the ratio of the $B_\perp$ and $B_\parallel$ scales. This has a simple interpretation if we notice that the relevant value of k_S is related, via the circulation theorem, to the magnetic flux Φ threading the Nb/InAs bilayer for given field orientation (Fig. 4b and c): $k_S = -\pi/W \times \Phi/\Phi_0$. Neglecting the field inhomogeneity in Nb,[21] we find $\Phi = B_\parallel W(d_S + d_N)$ and $\Phi = B_\perp W W_S$ for the parallel and perpendicular cases, respectively. Consequently, the expected field ratio is $B_\parallel/B_\perp = W_S/(d_S + d_N) = 20$, which is within the margins of the experimental uncertainty.

The dramatic reduction of the AR amplitude $a(B)$, inferred from the behavior of I_{exc}, can also explain the suppression of the higher lobes of the critical current in the Fraunhofer pattern in weak perpendicular magnetic field (see Fig. 1d), since the same $a(B)$ determines the energies of the ABS and hence $I_C(B)$.[12,13] We also note that the smaller the channel width W is, the higher are the values of $B_\perp$ required to reach $\Phi = \Phi_0$ in the junction and the stronger is the suppression of $I_C(B)$ at this point.

As a final check of consistency, we examined the critical current in a parallel magnetic field for samples #1 and #2a. Again we note that even for perfectly parallel field there is a phase gradient driven by the magnetic vector potential (Fig. 4b) that induces a Doppler energy shift of the ABS. When it becomes comparable to Γ_{McM}, counter-propagating ABS overlap in energy, which gradually cancels their contribution to the supercurrent. Similar to I_{exc}, the suppression of I_C occurs on the scale of $\simeq 100$ mT. In Fig. 5 we plot the variation of I_C of sample #1 with magnetic field for several almost parallel orientations. The small perpendicular component of $\mathbf{B}$ still leads to a Fraunhofer-like minimum in I_C, which allows a precise determination of the angle α between $\mathbf{B}$ and the junction's plane. This can be described by the expression $I_c(B) = I_c(B_\parallel)\,|\sin(\pi A B_\perp/\Phi_0)/(\pi A B_\perp/\Phi_0)|$,

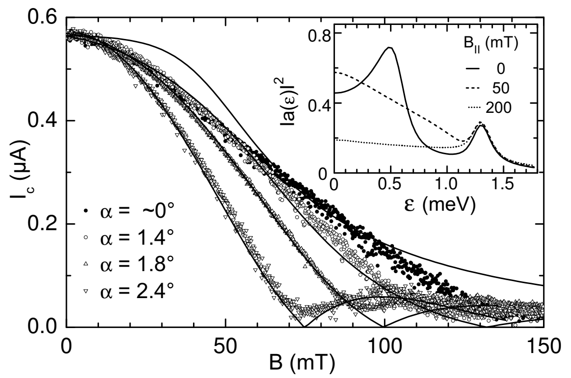

FIG. 5: Critical current vs. B of sample #1 for several small angles almost parallel to the 2DEG. The lines correspond to the best fits according to the theory (see text). The inset shows the double peak structure of $|a(\varepsilon)|^2$ characteristic for hybrid SC and its suppression by $B_{||}$.

where $B_\perp = B\sin\alpha$, $B_\parallel = B\cos\alpha$ and A is the junction's area. Unlike the standard Fraunhofer pattern,[11] we take into account the dependence of the critical current $I_c(B_\parallel)$ on the parallel component of the field. This is done by straightforward generalization of the ballistic formula for the Josephson current of Grajcar,[12] in which we express the AR amplitude a in terms of the McMillan's Green's functions with the Doppler shift in the InAs proximity layers. Because of the dependence $I_c(B_\parallel)$, the amplitude of the Fraunhofer-like oscillations decays much faster than the usual $1/B_\perp$ law, which is clearly seen in Fig. 5. For $\alpha \leq 1.3°$ no minimum is detected, while it is still observed for the wider sample #2a on the same chip (not shown). The curve for $\alpha \approx 0$ resulted from a careful maximization of I_C at fixed field, since in this case, evidently, no Fraunhofer minimum can be observed anymore. The solid lines in Fig. 5 are theoretical fits, when the effective thickness of the Nb/InAs bilayer, $d_{\rm eff}$ is varied. We find $d_{\rm eff} = d_N + d_S = 50$ nm for sample #2a (not shown) in agreement with the geometry, while for sample #1 $d_{\rm eff} \approx 25$ nm. The origin of this discrepancy is not clear, since the excess current data in Fig. 4 agree very well. The data for $\alpha = 0$ (i.e. $B_\perp = 0$) lie below the theoretical curve. This is probably caused by the perpendicular component of the weak stray field of the Nb electrodes.

In conclusion, we have investigated the IV-characteristics and the critical current of ballistic Nb/InAs Josephson junctions in parallel and perpendicular magnetic fields. The observed field dependence is much stronger than anticipated from standard models and can be traced back to the Doppler shift of Andreev levels induced by the diamagnetic supercurrents within the hybrid Nb/InAs contacts. Several different aspects of the proximity effect are consistently and nearly quantitatively described by our theoretical model.

We thank J. C. Cuevas and N. Shchelkachev for helpful discussions. The work was supported by the DFG (STR 438-2 and GRK 638).

---

* Present address: MPI-PKS, D-01187 Dresden, Germany.

1 I. O. Kulik, Zh. Eksp. Teor. Fiz. **57**, 1745 (1969) [Sov. Phys. JETP **30**, 944 (1970)].

2 For a review see, e.g., T. Schäpers, *Superconductor/Semiconductor Junctions* (Springer, Berlin, 2001), and the references therein.

3 P. E. Gregers-Hansen, E. Hendricks, M. T. Levinsen, and G. R. Pickett, Phys. Rev. Lett. **31**, 524 (1973); T. M. Klapwijk, G. E. Blonder, and M. Tinkham, Physica B & C **109/110**, 1657 (1982).

4 G. E. Blonder, M. Tinkham, and T. M. Klapwijk, Phys. Rev. B **25**, 4515 (1982).

5 C. Nguyen, H. Kroemer, and E. L. Hu, Phys. Rev. Lett. **69**, 2847 (1992); H. Takayanagi, T. Akazaki, and J. Nitta, Phys. Rev. Lett. **75**, 3533 (1995); J. P. Heida, B. J. van Wees, T. M. Klapwijk, and G. Borghs, Phys. Rev. B **60**, 13135 (1999); K. Neurohr *et al.*, Phys. Rev. B **59**, 11197 (1999).

6 H. Hoppe, U. Zülicke, and G. Schön, Phys. Rev. Lett. **84**, 1804 (2000).

7 J. Eroms *et al.*, Phys. Rev. Lett. **95**, 107001 (2005).

8 I. E. Batov *et al.*, Physical Review B **76** 115313 (2007).

9 J. Eroms *et al.*, Europhys. Lett. **58**, 569 (2002).

10 H. B. Heersche *et al.*, Nature **446**, 56 (2007).

11 M. Tinkham, *Introduction to Superconductivity* (McGraw-Hill, New York, 1996).

12 M. Grajcar *et al.*, Physica C **372**, 27 (2002).

13 P. W. Brouwer and C. W. J. Beenakker, Chaos, Solitons and Fractals **8**, 1249 (1997).

14 W. L. McMillan, Phys. Rev. **175**, 537 (1968).

15 A. A. Golubov and M. Yu. Kupriyanov, Physica C **259**, 27 (1996).

16 P. Samuelsson *et al.*, Phys. Rev. B**70**, 212505 (2004).

17 A. Chrestin, T. Matsuyama, and U. Merkt, Phys. Rev. B **55**, 8457 (1997).

18 S. Skalski, O. Betbeder-Matibet, and P. R. Weiss, Phys. Rev. **136**, A1500 (1964).

19 G. Tkachov and K. Richter, Phys. Rev. B **71**, 094517 (2005); G. Tkachov and V. I. Fal'ko, Phys. Rev. B **69**, 092503 (2004).

20 The Zeeman shift is 3-4 times smaller than ε_D.

21 This is justified, since, for the parallel field, the London penetration depth $\lambda_L \simeq 110$ nm is much larger than half of the Nb/InAs bilayer thickness $(d_S + d_N)/2 = 25$ nm, while, for the perpendicular field, the Pearl penetration depth $\lambda_P = 2\lambda_L^2/d_S \simeq 700$ nm is larger than half of the Nb stripe width $W_S/2 = 500$ mm.